In vitro evaluation of a hybrid drug delivery nanosystem for fibrosis prevention in type 1 diabetes cell therapy

1. Abstract (120 words):

Background: Implantation of insulin-secreting cells has been trialled as a treatment of type 1 diabetes mellitus (T1D), however the host immunogenic response limits their effectiveness.

Methodology: We developed the core-shell nanostructure of upconversion nanoparticle-mesoporous silica for controlled local delivery of an immuno-modulatory agent, MCC950, using near-infrared light and validated it using *in vitro* models of fibrosis.

Results: The individual components of the nanosystem did not affect proliferation of insulin-secreting cells unlike fibroblast proliferation ($p<0.01$). The nanosystem is effective at releasing MCC950 and preventing fibroblast differentiation ($p<0.01$), inflammation (IL-6 expression, $p<0.05$) and monocyte adhesion ($p<0.01$).

Conclusion: Our MCC950-loaded nanomedicine system could be used in the future together with insulin-secreting cell implants to increase their longevity as a curative treatment for T1D.

Plain language summary

Our study describes a new drug delivery system that can release an immunomodulatory drug in a controlled manner and prevent fibrosis that is part of the immune response when foreign body is implanted. This system can be particularly useful for insulin-secreting cell implants, used to replace multiple daily injections of insulin and improve the quality of life of people with type 1 diabetes mellitus (T1D). By preventing the immune response that leads to fibrosis, the longevity of these cellular implants can be extended without the need for frequent replacement procedures. We showed that our innovative nanosystem can release the required amount of an immunomodulatory drug, which could be stimulated with the use of special light, hence showing the ability for local and extended delivery. This type of system has the potential to reduce the side effects associated with oral daily administration of an immunomodulatory agents in people with T1D.

2. Lay abstract:

Tweetable abstract: In this article we describe an innovative approach for controlled release of immunomodulatory agent based on an upconversion nanomedicine system that could be explored for prevention of fibrosis of insulin-secreting cell implant treatment for type 1 diabetes mellitus.

Graphical abstract

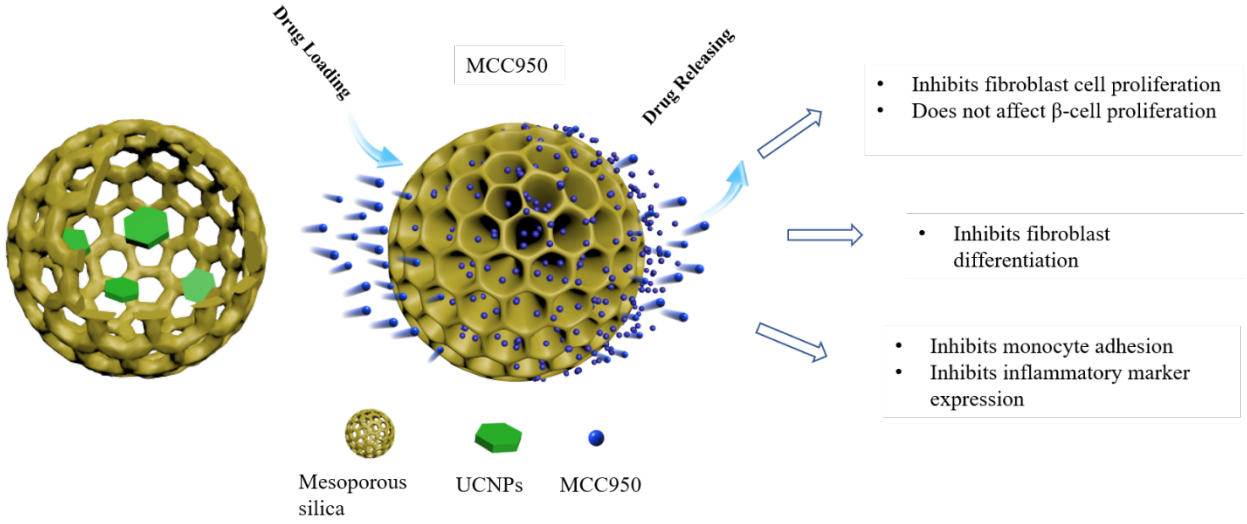

3. Keywords: 5—10 keywords that encapsulate the scope of the article.

Upconversion nanoparticles, mesoporous silica, fibrosis, immunomodulation, immune cells, fibroblasts

4. Introduction

Diabetes mellitus is one of the most serious and far-reaching chronic metabolic disorders globally, affecting 9.3% of the overall population [1]. Type 1 diabetes mellitus (T1D) is an autoimmune disease that affects people from a young age [2] and includes symptoms such as weight loss, polydipsia, polyuria and fatigue [3], and long term complications including nephropathy [4], cardiovascular disease [5], and limb amputations [6]. Currently, there are no curative treatments for T1D, with treatment predominantly relying on insulin replacement therapy through exogenous insulin administration and regular blood glucose monitoring[7]. Multiple daily subcutaneous injections of exogenous insulin can be labour intensive and uncomfortable hence affecting adversely the quality of life of people with T1D. Other alternatives exist including continuous glucose monitoring and insulin infusion devices,

which have shown to reduce the episodes of hypoglycaemia and improve blood glucose management [7]. Emerging treatments that could replace the use of insulin administration include cell replacement therapy, where insulin secreting cells are implanted, self-governing and maintaining glucose homeostasis. So far, there has been some success in developing islet cell replacement therapeutics for T1D with the first successful treatment being reported in 1980 where i) patients received an infusion of their own islet cells after pancreatectomy [8], ii) the development of the Edmonton protocol in 2000 for islet transplantation [9], and iii) the recent developments in stem cell engineering to create insulin-producing cells [10]. Unfortunately, there are still major hurdles to overcome with cell replacement therapies, the most pressing one being the scarcity of usable cells due to a lack of donors, in addition to low graft survival. In order to overcome this, many strategies are being utilised to generate insulin-producing cells from stem cells including nano- and micro-technology [11]. Hence, allogeneic insulin-secreting cell transplantation has emerged as a promising longer-term treatment for T1D [12]. Since the major challenges with this type of cell transplantation have been the viability of islet cells or immune rejection and hence long-term efficacy [13], encapsulation of the cells has been used to address these challenges and eliminate the need for the use of systemic immunosuppressive drugs that have many side effects [14]. However, the location of cell transplantation and invasiveness of these implanted cells still gives rise to immunogenic reactions. Traditionally, cells have been implanted into the liver or kidneys, however, other sites, such as bone marrow and muscle have been considered [15]. Recently, a bioartificial pancreas was transplanted into the abdominal aorta of rats [16]. Mridha *et al.* (2020) reported long term normalisation of blood glucose levels in non-obese diabetic/severe combined immunodeficient (NOD/SCID) mice using a subcutaneously implanted 3D scaffold containing alginate encapsulated insulin secreting cells [17]. Despite this, they reported that after 5 weeks, the scaffold and microencapsulated cells showed pro-inflammatory markers, macrophage adhesion and collagen deposition. Several clinical studies with encapsulated islets have shown limited long-term performance [18,19], and insulin independence is not routinely maintained [20] due to undesirable host immune response to the transplanted scaffolds [21]. The pores of the microcapsules within the subcutaneously implanted scaffolds become blocked as a result of fibrosis, and, after a few months, the inflow of nutrients and exit of insulin is inhibited [22,23], [24]. Consequently, an immunomodulatory agent (IMA) is needed to be delivered together with the transplanted insulin-producing cells to minimize host reactions and to maintain long-term function of the cell implants.

Smart nanomedicine systems with advanced and specific functionalities could improve the utility of cell-based therapies [25]. A range of nanomaterials has been developed as local immunomodulatory platforms to enhance targeted delivery, maintain drug stability and reduce toxicity and side effects.

Among the smart nanomedicine formulations using intrinsic stimuli, such as pH, enzyme, H_2O_2 and H_2S [26,27], and all types of external stimuli including magnetic and electronic field, thermal-/ultrasonic responses [23], light triggered smart nanomedicine systems present unique advantages in controllability, feasibility and modality [28,29]. Upconversion nanoparticles (UCNPs) that respond to near infrared (NIR) light stimulation are a strong candidate for smart nanomedicine as NIR has low risk of photodamage to tissues, deeper penetration depth, and it is highly feasible external stimulation compared to ultra-violet and visible lights [30-32]. UCNPs have been hybridized with mesoporous silica [33], polymers [34], hydrogel [35], ferric hydroxide [36], and ZnO [37] for precision nanomedicine applications mainly in cancer imaging and therapy with high efficacy.

The aim of this study was to show that our unique upconversion nanomedicine system can release MCC950 efficiently over time and prevent fibrosis towards a potential solution for addressing challenges with longevity and fibrosis development of insulin-secreting cell implants that are used as curative treatments for T1D. Herein, we adopted the core-shell nanostructure of UCNPs-mesoporous silica (MSN) to be the nanocarrier for an IMA, MCC950. The core-shell nanocarrier loaded with IMA and photo-responsive molecule aims to release the MCC950 upon NIR light irradiation. The controlled release of MCC950 would inhibit the host reaction to the microcapsules and maintain the functional capacity of the encapsulated insulin-producing cells. In this work, the biocompatibility of each component of the composite nanocarrier, including the UCNPS-MSN core-shell nanostructure, photo-responsive molecule, and MCC950, were assessed. The immunomodulatory effect of MCC950 and the MCC950-loaded in the nanocarrier were also demonstrated *in vitro* using fibroblast proliferation and differentiation, and monocyte adhesion assays. We also determined the MCC950 release profile with and without the NIR light irradiation. This work demonstrated the satisfactory safety of the smart upconversional nanomedicine system through the *in vitro* assessment, acceptable anti-fibrotic efficacy and improved drug release profile.

5. Materials & methods

5.1 Mesoporous particle synthesis

A method for the synthesis of AMS -6 has been described previously [38,38]. In this synthesis, the surfactant, *N*-Lauroyl-L-Alanine (1.25 g), was first added to 250 ml deionized water in a PVC bottle and kept in this bottle at 80℃ (400 rpm) for 12 hours. The surfactant solution was stirred for 10 min at 1000 rpm before adding a co-structure directing agent 3-aminopropyl triethoxysilane (APES, 1.25 g) and Tetraethyl orthosilicate (TEOS, 6.25 g) as the silica source. After addition, above solution was stirred at 1000 rpm for 1 hour. The speed was reduced to 500 rpm after 12 hours and the solution kept at RT for 12 hours without stirring. The as-synthesized AMS-6 material was filtered and dried overnight at RT; the surfactant was removed via calcination at 550 ℃ (3 hours in flowing air) to produce the final mesoporous particles.

5.2 Upconversion Nanoparticles (UCNPs) Synthesis

The typical synthesis procedure of $NaYF_4$: 20%Yb: 0.5%Er is as follows:[39,39,40] Lanthanide chloride (1 mmol), including YCl_3, $YbCl_3$ and $ErCl_3$, were dissolved in methanol at a molar ratio of 79.5:20:0.5 and then mixed with 6 ml of oleic acid and 15 ml of octadecene. In order to remove methanol and dissolve the lanthanide salts, the mixture was heated to 150 ℃ for 30 minutes. After cooling to room temperature, 2.5 mmol sodium hydroxide (NaOH) and 4 mmol ammonium fluoride (NH_4F) in methanol was added and stirred for another 30 minutes. The mixture was heated at 90 ℃ for 30 minutes and 150℃ for a further 10 minutes to evaporate the water and methanol. Subsequently, the reaction solution was heated to 300 ℃ for 90 minutes. The nanoparticles were washed using oleic acid, cyclohexane, methanol and ethanol mixture after the reaction solution was cooled to room temperature. Samples were dispersed in cyclohexane for further use.

5.3 Synthesis of the core-shell nanostructure of UCNPs - mesoporous silica

In this synthesis, the surfactant, *N*-Lauroyl-L-Alanine (0.14 g), and UCNPs (10 mg/ml, 2ml), was first added to 26 ml of deionized water in a PVC bottle and kept at 80 ℃ (400 rpm) for 12 hours. The surfactant solution was stirred for 10 min at 1000 rpm before adding a co-structure directing agent 3-aminopropyl triethoxysilane (965 µl APES) and TEOS (135 µl) as the silica source. After addition, the solution was stirred at 1000 rpm for 1 hour. The speed was reduced to 500 rpm after 12 hours

and the solutionmaintained at RT for 12 hours without stirring. The as-synthesized AMS-6 coating UCNPs (UCNPs-MSN) material was filtered and dried overnight at RT; the surfactant was removed by calcination at 400℃ (3 hours inflowing air) to produce the final particle.

5.4 In vitro drug release

5.4.1 MCC950 release into water

The core-shell structured mesoporous silica (UCNPs-MSN) containing photo-responsive molecules (hence forth referred to as the nanosystem) was loaded with MCC950 equivalent to 0.154 mg MCC950. The loaded nanosystem was added to 100 ml milli-Q water with constant stirring. The milli-Q water was used instead of physiological buffer solution because MCC950 is water soluble and therefore its integration into physiologically relevant solution is not a challenge in contrast to hydrophobic drugs. The nanosystems were stirred gently in water for 0.5 hrs to remove the MCC950 from the surfaces of nanosystems before solutions were sampled. Following this, the sample solutions were taken for analysis every half hour for the first 2 hours, and, then, every hour subsequently for the following 8 hours. This was repeated in a separate beaker with the water exposed to 980 nm near infrared (NIR) light for the total of 10 hrs. The NIR light was setup 30 cm above from the top surface of water and the power density of the NIR light was 2 w/cm^2.

5.4.2 MCC950 quantification via Liquid chromatography mass spectrometry (LC-MS/MS)

LC-MS/MS: The samples were analysed on Shimadzu LCMS-8060 Triple Quadrupole Mass spectrometer. The column oven was set to 40 °C, while the Autosampler was set to 15°C. 1µL of sample was injected onto a ZORBAX 300SB-C18 column (3.5 µm, 2.1 × 100 mm) at a flow rate of 0.3 ml/min using 0.1% formic acid in H2O (solvent A) and 100% acetonitrile (ACN; solvent B) as the gradient system. Chromatography was performed using the following gradient conditions: isocratic 2% B from 0 to 1 min, gradient 2% to 40% B from 1 to 2 mins, gradient 85% from 2 to 6 mins, isocratic 85% from 6 to 6.5 mins, gradient 85% to 2% B from 6.5 to 7.5 mins and isocratic 2% B from 7.5 to 10 mins. MS analyses were undertaken by Multiple Reaction Monitoring (MRM) mode using Turbo Spray (-)-ESI. MCC950 SRM parameters were determined by automated screening of parameters during infusion of a 1ppm solution of MCC950: Q1 402.6 to Q3 204.25 Da, dwell 100 msec, CE: 24, The peak areas from the MRM data for MCC950 were plotted in Microsoft Excel and the equation of

the line used to determine the MCC950 concentrations from the Area Under the Curve (AUC) for the 403.2 to 203.8 transition.

Preparation of standard curve: A 10 mM stock of MCC950 sodium salt (CP-456773 Sodium, Catalogue No.S7809) was prepared in water. 1ppm solution was prepared in 2% acetonitrile (ACN)+0.2% trifluoracetic acid in water. Serial dilutions from 1ppm (0.0333mM) to 0.00052 mM were prepared in the same solvent.

5.5 Determination of cell proliferation

Human fetal fibroblasts (HFF08) were seeded at 50,000 cells for 24 hrs in DMEM high glucose media (Thermofisher) with 10% foetal bovine serum (FBS) and 1% penicillin/streptomycin at 37°C and 5% CO_2. Following incubation, culture media was removed, cells washed and fresh media added containing treatments. Cell proliferation was determined by 2,5-diphenyl-2H-tetrazolium bromide (MTT) assay as per manufacturer's instructions, and colour intensity was measured at 570nm, with greater intensity indicating greater proliferation.

5.6 Fibroblast differentiation assay

Human fetal fibroblasts were seeded as above. The cells were then starved in DMEM/F12 (Thermofisher) containing 1% FBS and 1% penicillin/streptomycin for 24 h. Following this, fresh culture media containing 10ng/ml transforming growth factor (TGF)-β (Sigma-Aldrich), 10ng/ml TGF-β + 10nM/100nM/1μM MCC950 or 10ng/ml TGF-β + loaded nanosystem containing either 10nM/100nM/1μM MCC950, was added for 48h or 72h before protein or RNA was extracted for downstream analysis.

5.7 Protein expression analysis

5.7.1 Western blotting

Total protein was extracted from cell lysates and quantified using a Pierce™ BCA Protein Assay Kit (Thermo Fisher) as per the manufacturer's instruction. Protein lysates were loaded into Bio-Rad Protean Mini TGX gels and transferred using the Transblot Turbo System. Membranes before blocking the membrane in 5% skim milk and incubating it overnight at 4 °C in a primary antibody (Table 1). The following day, after membrane washing, the secondary antibody was added and the

membrane incubated for 2hrs at room temperature. Band intensity was determined using the FIJI software. Target protein expression was normalized to expression of the housekeeping protein (GAPDH).

5.7.2 Immunocytochemistry

Cells were seeded at 50,000 cells in a black 96-well plate. Following attachment, the cells were treated using the same conditions as described above for fibroblast differentiation assay, for 96 h. Cells were then fixed, blocked, and incubated overnight at 4°C in αSMA primary antibody (1:250, table 1) in blocking buffer. The following day, cells were incubated in secondary anti-rabbit AF488 and DAPI (1:1000) in blocking buffer before being imaged using the Nikon TiE2 inverted Fluorescence deconvolution microscope. Images of three random fields of view were taken per well. Images were analysed using the Fiji software and the percentage area stained determined.

5.8 Gene expression analysis

Total RNA was extracted using 1ml of TRISure (Bioline) as per the manufacturer's protocol. RNA was quantified using the NanoDrop 1000 (Thermo Scientific) and normalized to 200ng/µl. Samples were reverse transcribed to cDNA using the Tetro cDNA Synthesis Kit (Bioline) as per the manufacturer's instructions. Gene expression was quantified *via* qPCR using the SensiFast SYBR NO-ROX mix (Bioline). Primer sequences are listed in Table 2. Relative gene expression was calculated using the comparative analysis method as per the formula $2^{-\Delta\Delta Cq}$.

5.9 Cell adhesion

Fetal fibroblasts (HFF08) were seeded at 20,000 cells in 200µl of fibroblast culture media (FGM-2 SingleQuots, Lonza, CC-4126) in a black, clear bottom 96 well plate (Corning) at 37°C and 5% CO_2. Cells were allowed to adhere overnight, and then starved using the same starvation media as described above. The same treatment concentrations and time points were used as described above in the fibroblast differentiation assay.

In a separate flask, monocytes (THP-1 cells) were seeded and grown in RPMI 1640 media (Thermo Fisher) containing 10% FBS and 1% penicillin/streptomycin at 37°C and 5% CO_2. Cells were pelleted, washed, and resuspended at $2.5x10^4$ cells/ml in 10ml serum free RPMI media. The cell suspension

was spiked with Calcein AM dye (Thermo Fisher) prepared as per the manufacturer's instructions to give a final concentration of 2µM. The cells and dye were incubated at 37°C for 30mins.

Media containing treatments was removed from the seeded fibroblasts, fibroblasts were washed before the media was replaced with 200µl of RPMI media containing stained THP-1 cells. Cells were co-cultured for 30mins at 37°C and 5% CO_2. Following this incubation, non-adherent cells were removed by removing the media and washing. The fluorescent intensity was measured on the Infinite M1000 Pro at ex494nm/em517nm.

5.10 Data analysis

Data were tested for normality using the Shapiro-Wilks test. If data were determined to be normal, data was analysed using a One-way ANOVA. If data were determined to be not normally distributed, data was analysed using a multiple comparisons Kruskal-Wallis test. Data with repeated measures was analysed using mixed-model ANOVA. Data analysis was performed using GraphPad PRISM software.

6. Results

6.1 *In vitro* drug release with or without NIR light exposure

To determine the amount of drug being released from the mesoporous silica coated UCNPs (nanosystem), the nanosystem was loaded with known amounts of MCC950 and was soaked in water with constant stirring for 8 h. We also exposed the nanosystem to NIR light to stimulate MCC950 release. The amount of MCC950 released into solution was quantified using LC-MS/MS. Because the nanosystems were soaked in water and gently stirred for 0.5 hrs to remove the surface attached MCC950, the amount of the MCC9950 at the initial time point (0 h) was not zero. Overall, there was no significant difference in the total amount of MCC950 released from the nanosystem exposed to NIR light as compared to non-exposed UCNPs; the only significant difference between the two nanosystems was observed at 2h (Fig. 1). Although there was a trend towards the increased release amount of MCC950 following NIR exposure, further work is needed to confirm the results.

6.2 Cytotoxicity evaluation of the nanosystem components on murine insulin-producing cells and human fibroblasts

The composite drug nanosystem consists of mesoporous silica of AMS-6, photo-responsive molecules, UCNPs and MCC950, where UCNPs are coated within AMS-6 as an integrated core-shell nanostructure. In order to determine the cytotoxicity of these components on cells, the core-shell nanostructure, photo-responsive molecule and MCC950 were assessed at various concentrations by using two different types of cells: a murine pancreatic β cell line, MIN6, and human fibroblasts. Following 24 hour incubation, each component of the nanosystem within the concentration range (0.05 -1 mg/ml) did not affect cell proliferation. Interestingly, the photo-responsive molecule at 0.05mg/ml showed a significant increase in proliferation of MIN6 cells at 127.1%, (Fig. 2A; p=0.02). However, after a longer treatment of 48 h, proliferation of MIN6 cells was only significantly decreased to 75.8%, in the presence of the highest concentration of core-shell nanostructure tested, 1mg/ml (Fig. 2B; p=0.004), while all other components within the concentration range tested, did not adversely affect proliferation of MIN6 cells.

Conversely, in human fibroblasts (HFF08), proliferation was significantly reduced by every component of the nanosystem including MCC950 at almost every concentration tested after 48 hr treatment (Fig. 2C). Exposure to the photoresponsive molecule at the highest concentration of 1 mg/ml showed the lowest proliferation rate at 46.4%.

6.3 Effect of MCC950 and MCC950-loaded nanosystem on preventing fibroblast differentiation

In order to compare the effects of MCC950 and the MCC950-loaded nanosystem on preventing the differentiation of fibroblasts to myofibroblasts, which is a key process in fibrosis [41], the expression of alpha smooth muscle actin (α-SMA) was determined at both protein and RNA levels. This was measured upon exposure to a fibrotic stimulus, transforming growth factor beta (TGF-β), in the presence of various concentrations of MCC950-loaded nanosystem or MCC950 alone (Fig. 3). When we conducted immunostaining of the cells to determine the expression of α-SMA after 96 h, both MCC950 and the MCC950-loaded nanosystem at 100nM concentration, were capable of reducing the

expression of α-SMA (Fig. 3A; p=0.002, p=0.0005, respectively), indicative of fibrosis inhibition. Similarly, 1μM MCC950 significantly reduced α-SMA protein expression as compared to the TGF- β only stimulated cells (Fig. 3C, p=0.008); while the MCC950-loaded nanosystem containing the same concentration of the drug showed a trend towards reduction, although it was not statistically significant (p=0.07).

Furthermore, we determined α-SMA expression at the RNA level, following 48 and 72 h treatment, which showed significant upregulation of α-SMA gene expression following exposure to TGF- β at both timepoints confirming the presence of fibrosis (Fig. 3B&C; p<0.001). At 48 h, there was a trend towards α-SMA mRNA expression reduction, although not significantly, when treated with either 1μM MCC950 alone or the MCC950-loaded nanosystem. This trend was also observed with statistical significance when treatment was extended to 72 h, specifically in the presence of 1μM MCC950-loaded UCNPs (p=0.02).

6.4 Effect of MCC950 and the MCC950-loaded nanosystem on reducing IL-6 gene expression

The treatment of human fibroblasts using TGF-β significantly increased the gene expression of interleukin (IL)-6 at both 48 and 72h (P<0.0001; Fig. 4 A&B, respectively), confirming the presence of inflammation. At 48h, neither MCC950 alone nor the MCC950-loaded nanosystem could abrogate the increase in IL-6 mRNA expression induced by TGF- β. However, at 72h, both the higher concentrations of MCC950 alone and the MCC950-loaded nanosystem significantly decreased IL-6 expression as compared to TGF-β alone stimulated cells, demonstrating that the MCC950-loaded nanosystem can release the MCC950 consistently and prevent fibrosis (Fig. 4B; MCC950-loaded nanosystem [100nM], p=0.04; MCC950 [1μM], p<0.0001; MCC950-loaded nanosystem [1 μM], p<0.0001).

6.5 High concentrations of MCC950 and the MCC950-loaded nanosystem reduce macrophage adhesion

Finally, to support our findings presented above that our nanosystem loaded with MCC950 can release MCC950 consistently and prevent fibrosis, we conducted a functional assay to determine the ability of MCC950 loaded nanosystem to prevent macrophage adhesion to fibroblasts. Previous data with insulin-secreting cell implants showed that after several months, the implants become infiltrated with macrophages, enhancing the immune response, hence preventing the secretion of insulin by implanted insulin-secreted cells [17]. As such, we sought to determine whether MCC950 and loaded nanosystem could prevent the attachment of macrophages after stimulation with TGF-β. Following 48 h of stimulation with TGF-β in the presence of MCC950 or the MCC950-loaded nanosystem, there is a slight downward trend, as concentration of the treatment increased, in macrophage adhesion, compared to TGF-β treatment alone (Fig. 5A; p= 0.19 vs. MCC950 [1μM]; p=0.15 vs. MCC950-loaded nanosystem [1μM]). Statistical significance was only reached after 72 h treatment in cells stimulated with TGF-β in the presence of MCC950-loaded nanosystem (1μM) compared to TGF-β alone (Fig. 5B; p=0.007).

7. Discussion

Overall, we have demonstrated that our innovative MCC950-loaded nanosystem can successfully release loaded drug over time. Moreover, when exposed to NIR light, the amount released is slightly enhanced although not statistically significant except at 2 h time point; the overall trend showing the increased release rate. We have also shown that this drug-loaded nanosystem prevents fibrosis via the comprehensive *in vitro* evaluations. The results demonstrate reduction in (i) fibroblast to myofibroblast differentiation, (ii) α-SMA and IL-6 gene expression and (iii) immune cell adhesion. These are all important processes in fibrosis development of implants containing cell-based therapies [42,43].

It is detrimental for an implant containing insulin-secreting cells for treatment of T1D to evade immune reaction, where fibroblast attachment to the microcapsules containing insulin-secreting cells prevents the excretion of insulin. We demonstrated that treatment with our innovative drug delivery nanosystem, *in vitro,* could potentially overcome fibrosis, which may translate into prevention of immunogenic response to cell-containing implant that should be tested *in vivo* in the

future. Interestingly, we demonstrated that each of the components of our nanosystem reduce fibroblast proliferation, while overall not having an inhibitory effect on murine β-islet cells except with the highest concentration of UCNPs-MS following 48 h treatment. However, given that Min6 cells are not a pure beta cell line, this experiment should be repeated in the future using primary islets. Furthermore, whether individual components affect insulin secretion from islets should be determined in the future when the nanosystem is combined with insulin-secreting cells.

MCC950 is a well-established anti-inflammatory molecule that non-covalently binds to the Walker B site on NLRP3 preventing structural conformational change of the ATP-binding site, thereby preventing assembly of the NOD-like receptor protein-3 (NLRP3) inflammasome [44,45]. By preventing the assembly, MCC950 prevents the activation of mature interleukin (IL)-1β, IL-18 and caspase 1 [4546]. Given the pro-inflammatory response to the insulin-secreting cell-containing implants reported previously [46], MCC950 is an attractive candidate for loading into this nanosystem as a proof of concept for prevention of inflammation and subsequently fibrosis to improve cell implant longevity. However, the dual response of inflammation and fibrosis dictates that the nanosystem should be loaded with a drug that can be both anti-inflammatory, as well as anti-fibrotic [47,48]. Several studies have recently been undertaken to determine the effect of MCC950 on fibrosis *in vivo* [49-51], however, given the close relationship between inflammation and fibrosis development, it is difficult to determine whether resolution/reduction of fibrosis is due to a direct effect of MCC950 or due to MCC950's ability to reduce inflammation. Additionally, these models focus primarily on heart and liver diseases. Therefore, in this study we determined MCC950's direct effect on fibroblasts without inflammatory stimulation. TGF-β is a central regulator of fibrosis, which stimulates the differentiation of fibroblasts to myofibroblasts [47]. Myofibroblasts secrete matrix proteins, including alpha smooth muscle actin (αSMA) [47,48]. We demonstrated that at longer timepoints, such as 96 h, the co-treatment with TGF- β and high concentrations of both MCC950 and the MCC950-loaded nanosystem, reduced protein αSMA expression. Further, we showed that gene expression of αSMA was only significantly reduced following 72 h treatment and not 48 h, and only with MCC950-loaded nanosystem rather than MCC950 alone, although there was a strong trend. This suggests that sustained treatment with MCC950 or the MCC950-loaded UCNPs is required to reduce translation of

gene expression to protein expression as demonstrated by reduction in αSMA protein abundance measured by immunohistochemistry.

While the NLRP3 inflammasome has been shown to stimulate TGF-β [52] and TGF-β is also known to have anti-inflammatory effects [53], given that it is already well established that MCC950 is an inhibitor of the inflammasome assembly, and prevents activation of interleukin (IL)-18, IL-1 β and caspase-1 we did not assess the effects of MCC950 or MCC950-loaded nanosystem on these markers. However, there is a cross talk between TGF-β and IL-6 *via* positive and negative feedback loops where the addition of IL-6 and TGF-β increases the expression of the other [54]. TGF-β attenuated the effects of IL-6 [55], while IL-6 has been shown to promote TGF-β [56]. We have shown that TGF-β stimulation increased gene expression of IL-6, and following a longer treatment for 72 h, MCC950 and MCC950-loaded nanosystem reduced gene expression of IL-6 in cells stimulated with TGF-β.

Finally, since TGF-β acts at a chemoattractant for monocytes [57], a functional monocyte adhesion assay was performed to determine the ability of MCC950 and MCC950-loaded nanosystem to prevent the attachment of monocytes to fibroblasts. We confirmed our findings that MCC950-loaded nanosystem can prevent monocyte adhesion to fibroblasts whilst also inhibiting IL-6 gene expression and αSMA expression. Similarly, this was only observed following 72 h treatment and with MCC950-loaded nanosystem and not MCC950 alone, suggesting a more potent effect on fibrosis when MCC950 was loaded within our nanosystem.

Future direction for this work towards translation should include further optimisation of NIR-stimulated release of MCC950 from this upconversion nanosystem over a longer period of time. Incorporation of the immunomodulatory agent-containing nanosystem with insulin-secreting cell implants should also be evaluated in terms of the impact on the islets and the ability of the nanosystem to prevent or delay the development of perivascular growth on the implants *in vivo* using diabetic mouse models. Once the preclinical testing is completed showing safety and efficacy, the system could be potentially moved into clinical trials.

8. Conclusion

In summary, we have developed a novel nanosystem that can efficiently release an immunomodulatory agent over extended time period capable of preventing early processes of fibrosis. We demonstrated *in vitro* the release profile of MCC950 from this nanosystem that could potentially be stimulated with the NIR light irradiation in the future towards controlled drug release. MCC950-loaded nanosystem was able to downregulate pro-fibrotic markers, αSMA and IL-6, and reduce monocyte adhesion to fibroblasts. This could be beneficial in the future in preventing perivascular growth from cell-containing implants particularly in the area of T1D treatment.

9. Future Perspective:

- (a speculative viewpoint on how the field will evolve in 5–10 years' time)

Whilst transformational curative treatments for T1D have been developed and used clinically, their longevity and efficacy has been impeded by the immunogenic response observed *in vivo* that leads to fibrosis of the implanted β cells, hence limiting their use. To address this challenge, we developed an innovative nanosystem that can successfully load and release an immunomodulating agent and prevent early processes of fibrosis with a potential to increase longevity of implanted β cells. This may improve the management of blood glucose and quality of life of people with type 1 diabetes mellitus.

10. Executive Summary:

- (bulleted summary points that illustrate the main conclusions made throughout the article. Less than 400 words).

OR

11. Summary Points (Research articles & Company profiles only):

8–10 bullet point sentences highlighting the key points of the article.

- We designed an innovative nanosystem capable of releasing an immunomodulatory agent, MCC950, over a prolonged period of time.
- Although various components of the nanosystem were not overall toxic to murine β cells except at the very high doses, these were toxic to fetal fibroblast cells.
- MCC950 released from the nanosystem inhibited the expression of fibrotic markers, α-SMA and IL-6 following longer treatment over 72-96h.
- Released MCC950 also inhibited monocyte adhesion to fibroblasts, one of the key processes in the development of fibrosis.
- Controlled release of MCC950 from the nanosystem could potentially be achieved in the future using near-infrared light irradiation; however this needs further optimisation.
- Our MCC950-loaded nanomedicine system could be used in the future together with insulin-secreting cell implants to increase efficacy and longevity of this treatment for type 1 diabetes mellitus.

12. Figure/Table legends

Figure 1: Drug release from our nanomedicine system. Drug release into water from free UCNPs with and without exposure to NIR was quantified *via* LCMS. Statistical significance was determined *via* mixed effects analysis. Results are presented as Mean ± SEM.

Figure 2: The effect of various components of the nanomedicine system on cell proliferation. Cell proliferation when exposed to components of the UCNPs was determined via an MTT assay using Min6 cells for 24hrs (A) and 48hrs (B), as well as human fetal fibroblasts (C). N=3-4. Statistical significance was determined via One-way ANOVA or Kruskal-Wallis tests. Results are presented as Mean ± SEM. *P<0.05, **P<0.01, ***P<0.001, ****P<0.0001 vs untreated.

Figure 3: Differentiation of Fibroblasts. Human fetal fibroblast differentiation following treatment with 10ng/ml TGF-β with or without MCC950 alone or MCC950-loaded nanosystem. (A) Expression of αSMA at 96hrs was quantified *via* immunocytochemistry. αSMA gene expression was quantified via qPCR at 48 and 72hrs (B&C, respectively). N≥3. Statistical significance was determined *via* One-way ANOVA or Kruskal-Wallis tests. Results are presented as Mean ± SEM. *P<0.05, **P<0.01, ***P<0.001, ****P<0.0001.

Figure 4: IL-6 gene expression. Human fibroblast were exposed to 10ng/ml TGF-β and an MCC950 treatment. RNA was extracted and expression of IL-6 at 48 (A) and 72hrs (B) was quantified *via* qPCR (A&B, respectively). N=4. Statistical significance was determined *via* One-way ANOVA or Kruskal-Wallis tests. Results are presented as Mean ± SEM. *P<0.05, ****P<0.0001**.**

Figure 5: Macrophage adhesion to stimulated fibroblasts. Human fibroblast were exposed to 10ng/ml TGF-β and an MCC950 treatment for 48hrs (A) or 72hrs (B). Stained THP-1 cells were cocultured with treated fibroblasts and allowed to attach. Following washing to remove non-adherent cells, fluorescence of adherent cells was quantified *via* spectroscopy. N=5. Statistical significance was determined *via* One-way ANOVA. Results are presented as Mean ± SEM. **P<0.01 vs. untreated.

Table 1: Antibodies used for western blot analysis

Target	Dilution	Catalogue number
GAPDH	1:5000 (Western blot)	ab37168
αSMA	1:5000 (Western blot) 1:250 (ICC)	ab124964
Anti-rabbit secondary	1:10,000 (Western blot)	7074P2
Anti-rabbit secondary AF 488	1:750 (ICC)	ab150077

Table 2: Primer sequences for gene expression analysis

Gene	Forward sequence	Reverse sequence
αSMA/ACTA2	5'-AGATCAAGATCATTGCCCC	5'-TTCATCGTATTCCTGTTTGC
IL-6	5'-AAGATTCCAAAGATGTAGCC	5'-ACATGTCTCCTTTCTCAGG

13. Author contributions

CR performed the experiments, data analysis and wrote the manuscript. YH, PS, ZD, MP contributed to the experimental design and performance. BET, XX and LM conceived the study design or made significant contribution to the study design, data analysis and/or interpretation and manuscript writing. XX and LM conceived the study, designed the experiments, supervised CR, YH and PS, wrote the manuscript. All authors reviewed and approved the final manuscript.

14. Acknowledgements

n/a

15. Disclosures

The work was funded by a JDRF Innovative Grant (1-INO-2020-914-A).

16. Ethical conduct of research

n/a

17. Data sharing statement

The data that support the findings of this study are available on reasonable request from the corresponding authors, LM and XX.

18. References:

1. Saeedi, P., *et al.* Global and regional diabetes prevalence estimates for 2019 and projections for 2030 and 2045: Results from the International Diabetes Federation Diabetes Atlas, 9th edition. *Diabetes Research and Clinical Practice* **157**(2019).
2. Ever-Increasing Insulin-Requiring Patients Globally. *Diabetes Technology & Therapeutics* **20**, S2-1-S2-4 (2018).
3. Ramachandran, A. Know the signs and symptoms of diabetes. *Indian J Med Res* **140**, 579-581 (2014).

4. Chawla, A., Chawla, R. & Jaggi, S. Microvasular and macrovascular complications in diabetes mellitus: Distinct or continuum? *Indian Journal of Endocrinology and Metabolism* **20**, 546-551 (2016).
5. Schofield, J., Ho, J. & Soran, H. Cardiovascular Risk in Type 1 Diabetes Mellitus. *Diabetes Ther* **10**, 773-789 (2019).
6. Déruaz-Luyet, A., Raabe, C., Garry, E.M., Brodovicz, K.G. & Lavery, L.A. Incidence of lower extremity amputations among patients with type 1 and type 2 diabetes in the United States from 2010 to 2014. *Diabetes, Obesity and Metabolism* **22**, 1132-1140 (2020).
7. Pathak, V., Pathak, N.M., O'Neill, C.L., Guduric-Fuchs, J. & Medina, R.J. Therapies for Type 1 Diabetes: Current Scenario and Future Perspectives. *Clin Med Insights Endocrinol Diabetes* **12**, 1179551419844521-1179551419844521 (2019).
8. Sutherland, D.E., Matas, A.J., Goetz, F.C. & Najarian, J.S. Transplantation of dispersed pancreatic islet tissue in humans: autografts and allografts. *Diabetes* **29 Suppl 1**, 31-44 (1980).
9. Shapiro, A.M.*, et al.* Islet transplantation in seven patients with type 1 diabetes mellitus using a glucocorticoid-free immunosuppressive regimen. *N Engl J Med* **343**, 230-238 (2000).
10. Chen, S., Du, K. & Zou, C. Current progress in stem cell therapy for type 1 diabetes mellitus. *Stem Cell Research & Therapy* **11**, 275 (2020).
11. Mooranian, A.*, et al.* Advanced bile acid-based multi-compartmental microencapsulated pancreatic β-cells integrating a polyelectrolyte-bile acid formulation, for diabetes treatment. *Artif Cells Nanomed Biotechnol* **44**, 588-595 (2016).
12. Wang, H.S.*, et al.* Transplantation of insulin-producing cells derived from umbilical cord stromal mesenchymal stem cells to treat NOD mice. *Cell Transplant* **20**, 455-466 (2011).
13. Gamble, A., Pepper, A.R., Bruni, A. & Shapiro, A.M.J. The journey of islet cell transplantation and future development. *Islets* **10**, 80-94 (2018).
14. Opara, E.C., McQuilling, J.P. & Farney, A.C. Microencapsulation of pancreatic islets for use in a bioartificial pancreas. *Methods Mol Biol* **1001**, 261-266 (2013).
15. Addison, P., Fatakhova, K. & Rodriguez Rilo, H.L. Considerations for an Alternative Site of Islet Cell Transplantation. *J Diabetes Sci Technol* **14**, 338-344 (2020).
16. Han, E.X.*, et al.* Development of a Bioartificial Vascular Pancreas. *J Tissue Eng* **12**, 20417314211027714 (2021).
17. Prevascularized Retrievable Hybrid Implant to Enhance Function of Subcutaneous Encapsulated Islets. *Tissue Engineering Part A* **0**, null.
18. Tuch, B.E.*, et al.* Safety and Viability of Microencapsulated Human Islets Transplanted Into Diabetic Humans. *Diabetes Care* **32**, 1887-1889 (2009).
19. Basta, G.*, et al.* Long-Term Metabolic and Immunological Follow-Up of Nonimmunosuppressed Patients With Type 1 Diabetes Treated With Microencapsulated Islet Allografts: Four cases. *Diabetes Care* **34**, 2406-2409 (2011).

20. Vaithilingam, V., Bal, S. & Tuch, B.E. Encapsulated Islet Transplantation: Where Do We Stand? *Rev Diabet Stud* **14**, 51-78 (2017).
21. Veiseh, O.*, et al.* Size- and shape-dependent foreign body immune response to materials implanted in rodents and non-human primates. *Nature Materials* **14**, 643-651 (2015).
22. Bochenek, M.A.*, et al.* Alginate encapsulation as long-term immune protection of allogeneic pancreatic islet cells transplanted into the omental bursa of macaques. *Nature Biomedical Engineering* **2**, 810-821 (2018).
23. Lopez-Mendez, T.B., Santos-Vizcaino, E., Pedraz, J.L., Orive, G. & Hernandez, R.M. Cell microencapsulation technologies for sustained drug delivery: Latest advances in efficacy and biosafety. *Journal of Controlled Release* **335**, 619-636 (2021).
24. Mridha A, C.L., Morris M, Vaithilingam V, Dargaville TR, Tuch B. Immunosupppression free allogeneic beta cell therapy for type-1-diabetes using an Australian bioengineered device. in *Australasian Diabetes Congress* (Adelaide, Australia, 2018).
25. Germain, M.*, et al.* Delivering the power of nanomedicine to patients today. *J Control Release* **326**, 164-171 (2020).
26. Li, Y., An, L., Lin, J., Tian, Q. & Yang, S. Smart nanomedicine agents for cancer, triggered by pH, glutathione, H(2)O(2), or H(2)S. *Int J Nanomedicine* **14**, 5729-5749 (2019).
27. Mura, S., Nicolas, J. & Couvreur, P. Stimuli-responsive nanocarriers for drug delivery. *Nature Materials* **12**, 991-1003 (2013).
28. Zhao, P.*, et al.* NIR-driven Smart Theranostic Nanomedicine for On-demand Drug Release and Synergistic Antitumour Therapy. *Scientific Reports* **5**, 14258 (2015).
29. Kim, J., Jo, Y.-u. & Na, K. Photodynamic therapy with smart nanomedicine. *Archives of Pharmacal Research* **43**, 22-31 (2020).
30. Yang, D.*, et al.* Current advances in lanthanide ion (Ln3+)-based upconversion nanomaterials for drug delivery. *Chemical Society Reviews* **44**, 1416-1448 (2015).
31. Jalani, G., Tam, V., Vetrone, F. & Cerruti, M. Seeing, Targeting and Delivering with Upconverting Nanoparticles. *Journal of the American Chemical Society* **140**, 10923-10931 (2018).
32. Lee, G. & Park, Y.I. Lanthanide-Doped Upconversion Nanocarriers for Drug and Gene Delivery. *Nanomaterials (Basel)* **8**(2018).
33. Zhao, L.*, et al.* Near-Infrared Photoregulated Drug Release in Living Tumor Tissue via Yolk-Shell Upconversion Nanocages. *Advanced Functional Materials* **24**, 363-371 (2014).
34. Liu, J.*, et al.* Light-controlled drug release from singlet-oxygen sensitive nanoscale coordination polymers enabling cancer combination therapy. *Biomaterials* **146**, 40-48 (2017).
35. Jalani, G.*, et al.* Photocleavable Hydrogel-Coated Upconverting Nanoparticles: A Multifunctional Theranostic Platform for NIR Imaging and On-Demand Macromolecular Delivery. *Journal of the American Chemical Society* **138**, 1078-1083 (2016).

36. Wu, X., *et al.* Ferric Hydroxide-Modified Upconversion Nanoparticles for 808 nm NIR-Triggered Synergetic Tumor Therapy with Hypoxia Modulation. *ACS Applied Materials & Interfaces* **11**, 385-393 (2019).
37. Wang, Y., Song, S., Liu, J., Liu, D. & Zhang, H. ZnO-Functionalized Upconverting Nanotheranostic Agent: Multi-Modality Imaging-Guided Chemotherapy with On-Demand Drug Release Triggered by pH. *Angewandte Chemie International Edition* **54**, 536-540 (2015).
38. Atluri, R., Hedin, N. & Garcia-Bennett, A.E. Hydrothermal phase transformation of bicontinuous cubic mesoporous material AMS-6. *Chemistry of Materials* **20**, 3857-3866 (2008).
39. Liu, D., *et al.* Three-dimensional controlled growth of monodisperse sub-50 nm heterogeneous nanocrystals. *Nature communications* **7**, 1-8 (2016).
40. Liu, D., *et al.* Emission stability and reversibility of upconversion nanocrystals. *Journal of Materials Chemistry C* **4**, 9227-9234 (2016).
41. Hinz, B. Myofibroblasts. *Exp Eye Res* **142**, 56-70 (2016).
42. Tomei, A.A., Villa, C. & Ricordi, C. Development of an encapsulated stem cell-based therapy for diabetes. *Expert opinion on biological therapy* **15**, 1321-1336 (2015).
43. Johnson, B.Z., Stevenson, A.W., Prêle, C.M., Fear, M.W. & Wood, F.M. The Role of IL-6 in Skin Fibrosis and Cutaneous Wound Healing. *Biomedicines* **8**(2020).
44. Coll, R.C., *et al.* A small-molecule inhibitor of the NLRP3 inflammasome for the treatment of inflammatory diseases. *Nat Med* **21**, 248-255 (2015).
45. El-Sharkawy, L.Y., Brough, D. & Freeman, S. Inhibiting the NLRP3 Inflammasome. *Molecules* **25**, 5533 (2020).
46. Mridha, A.R., *et al.* Prevascularized Retrievable Hybrid Implant to Enhance Function of Subcutaneous Encapsulated Islets. *Tissue Eng Part A* **28**, 212-224 (2022).
47. Biernacka, A., Dobaczewski, M. & Frangogiannis, N.G. TGF-β signaling in fibrosis. *Growth Factors* **29**, 196-202 (2011).
48. Fielding, Ceri A., *et al.* Interleukin-6 Signaling Drives Fibrosis in Unresolved Inflammation. *Immunity* **40**, 40-50 (2014).
49. Gao, R., *et al.* The selective NLRP3-inflammasome inhibitor MCC950 reduces myocardial fibrosis and improves cardiac remodeling in a mouse model of myocardial infarction. *International Immunopharmacology* **74**, 105575 (2019).
50. Qu, J., Yuan, Z., Wang, G., Wang, X. & Li, K. The selective NLRP3 inflammasome inhibitor MCC950 alleviates cholestatic liver injury and fibrosis in mice. *International Immunopharmacology* **70**, 147-155 (2019).
51. Mridha, A.R., *et al.* NLRP3 inflammasome blockade reduces liver inflammation and fibrosis in experimental NASH in mice. *Journal of Hepatology* **66**, 1037-1046 (2017).
52. Wang, W., *et al.* Inflammasome-Independent NLRP3 Augments TGF-β Signaling in Kidney Epithelium. *The Journal of Immunology* **190**, 1239-1249 (2013).
53. Alyaseer, A.A.A., de Lima, M.H.S. & Braga, T.T. The Role of NLRP3 Inflammasome Activation in the Epithelial to Mesenchymal Transition Process During the Fibrosis. *Front Immunol* **11**, 883-883 (2020).

54. Yamada, D*., et al.* Role of crosstalk between interleukin-6 and transforming growth factor-beta 1 in epithelial–mesenchymal transition and chemoresistance in biliary tract cancer. *European Journal of Cancer* **49**, 1725-1740 (2013).
55. Srivastava, A*., et al.* Interleukin-6 Induced Proliferation Is Attenuated by Transforming Growth Factor-β-Induced Signaling in Human Hepatocellular Carcinoma Cells. *Frontiers in Oncology* **11**(2022).
56. Luckett-Chastain, L.R. & Gallucci, R.M. Interleukin (IL)-6 modulates transforming growth factor-beta expression in skin and dermal fibroblasts from IL-6-deficient mice. *Br J Dermatol* **161**, 237-248 (2009).
57. Li, M.O., Wan, Y.Y., Sanjabi, S., Robertson, A.-K.L. & Flavell, R.A. TRANSFORMING GROWTH FACTOR-β REGULATION OF IMMUNE RESPONSES. *Annual Review of Immunology* **24**, 99-146 (2006).

607

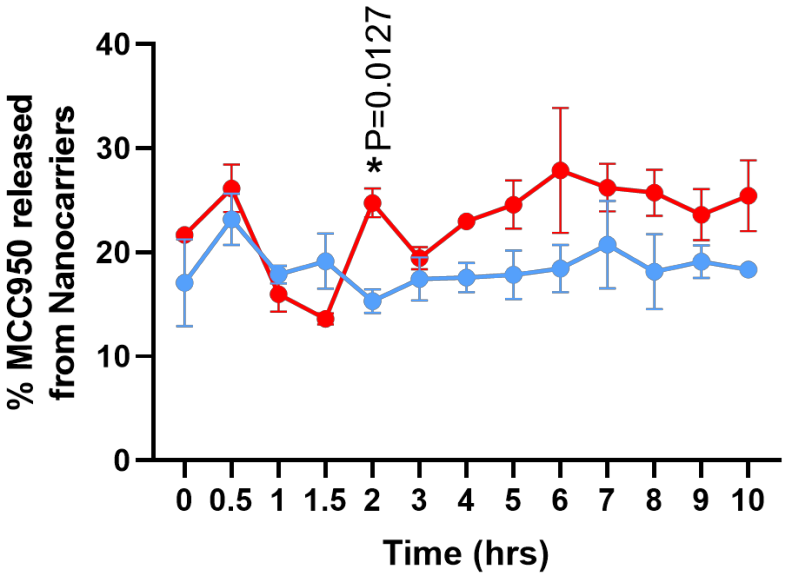

608

609

610

611

612

613

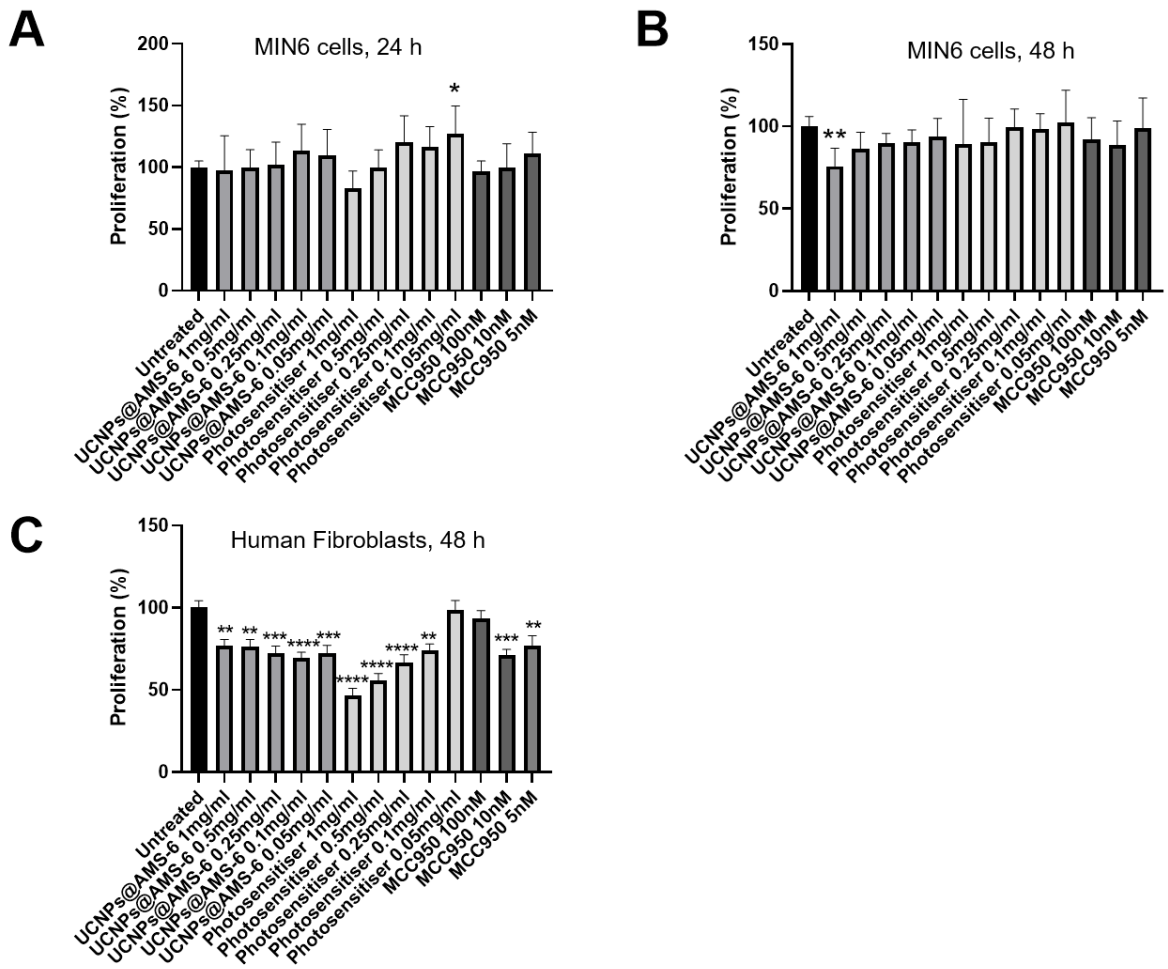
A
MIN6 cells, 24 h
Proliferation (%)
200
150
100
50
0
*
B
MIN6 cells, 48 h
Proliferation (%)
150
100
50
0
**
C
Human Fibroblasts, 48 h
Proliferation (%)
150
100
50
0
Untreated
UCNPs@AMS-6 1mg/ml
UCNPs@AMS-6 0.5mg/ml
UCNPs@AMS-6 0.25mg/ml
UCNPs@AMS-6 0.1mg/ml
UCNPs@AMS-6 0.05mg/ml
Photosensitiser 1mg/ml
Photosensitiser 0.5mg/ml
Photosensitiser 0.25mg/ml
Photosensitiser 0.1mg/ml
Photosensitiser 0.05mg/ml
MCC950 100nM
MCC950 10nM
MCC950 5nM

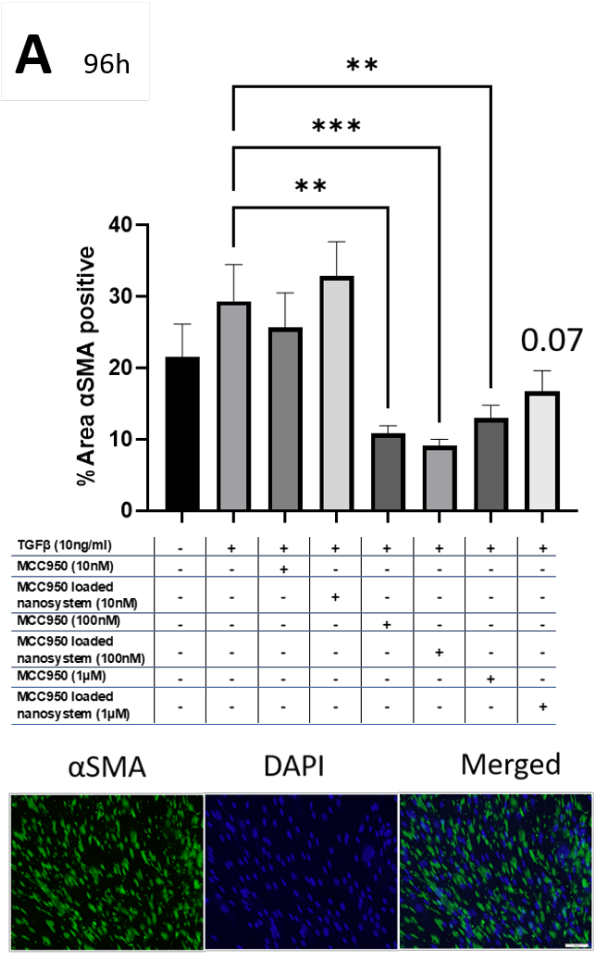
A 96h
**
***
**
% Area αSMA positive
40
30
20
10
0
0.07
TGFβ (10ng/ml)
MCC950 (10nM)
MCC950 loaded nanosystem (10nM)
MCC950 (100nM)
MCC950 loaded nanosystem (100nM)
MCC950 (1μM)
MCC950 loaded nanosystem (1μM)
αSMA
DAPI
Merged

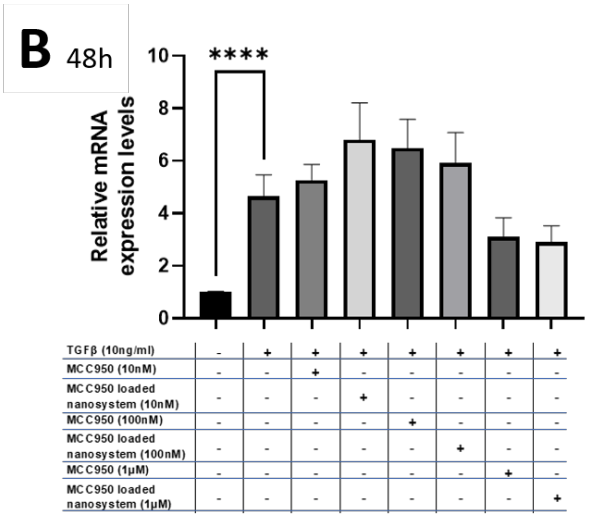
B 48h
****
Relative mRNA expression levels
10
8
6
4
2
0
TGFβ (10ng/ml)
MCC950 (10nM)
MCC950 loaded nanosystem (10nM)
MCC950 (100nM)
MCC950 loaded nanosystem (100nM)
MCC950 (1μM)
MCC950 loaded nanosystem (1μM)

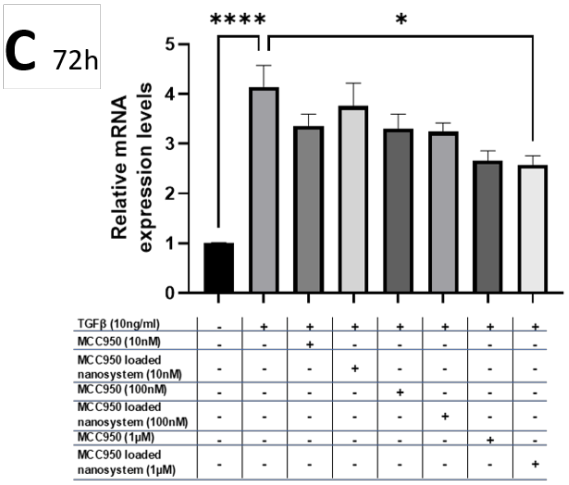
C 72h
****
*
Relative mRNA expression levels
5
4
3
2
1
0
TGFβ (10ng/ml)
MCC950 (10nM)
MCC950 loaded nanosystem (10nM)
MCC950 (100nM)
MCC950 loaded nanosystem (100nM)
MCC950 (1μM)
MCC950 loaded nanosystem (1μM)

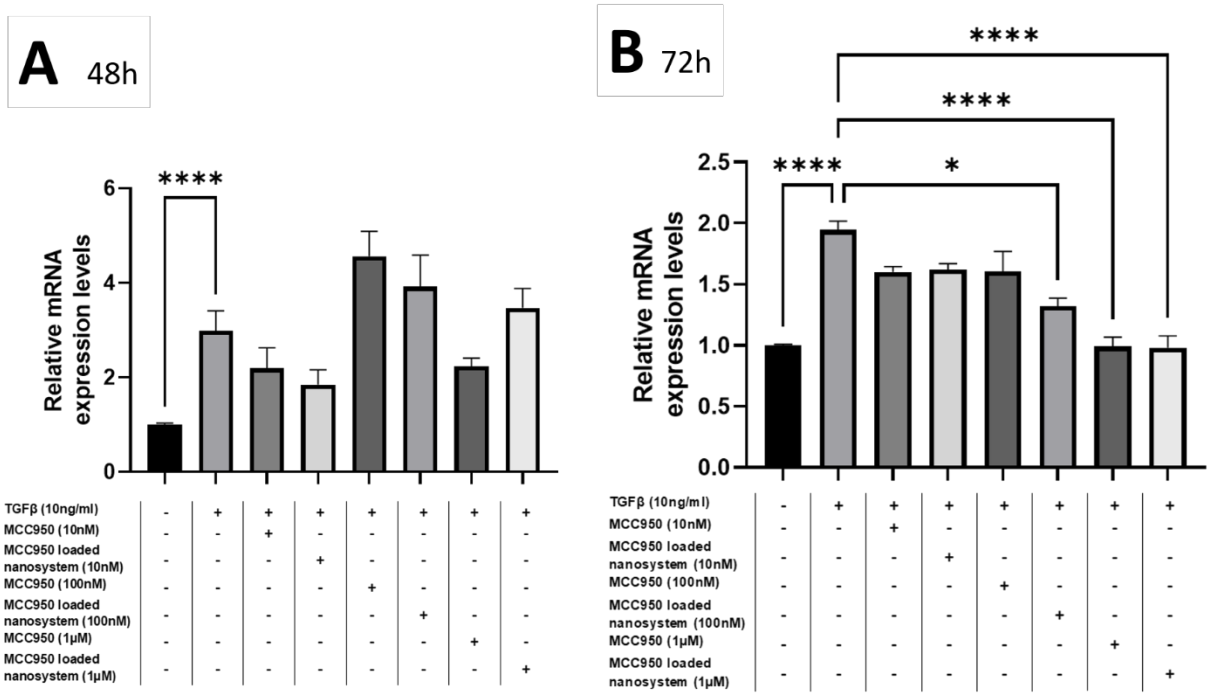
A 48h
****
Relative mRNA expression levels
6
4
2
0
TGFβ (10ng/ml)
MCC950 (10nM)
MCC950 loaded nanosystem (10nM)
MCC950 (100nM)
MCC950 loaded nanosystem (100nM)
MCC950 (1μM)
MCC950 loaded nanosystem (1μM)
B 72h
****
****
****
*
Relative mRNA expression levels
2.5
2.0
1.5
1.0
0.5
0.0
TGFβ (10ng/ml)
MCC950 (10nM)
MCC950 loaded nanosystem (10nM)
MCC950 (100nM)
MCC950 loaded nanosystem (100nM)
MCC950 (1μM)
MCC950 loaded nanosystem (1μM)

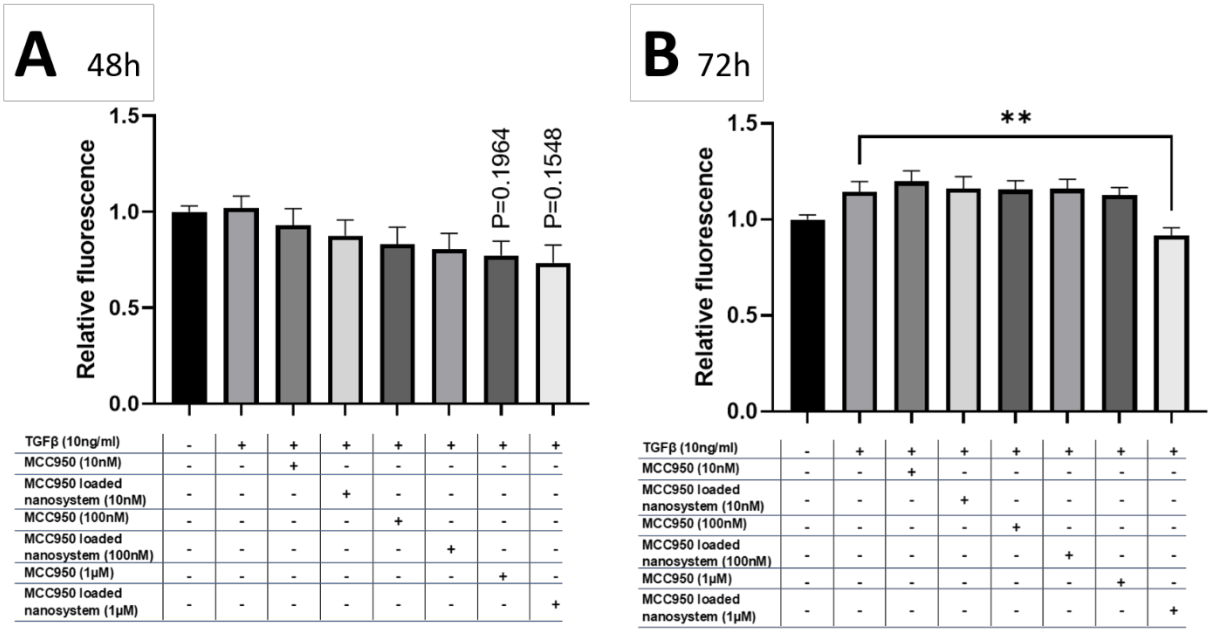
A 48h
Relative fluorescence
1.5
1.0
0.5
0.0
P=0.1964
P=0.1548
TGFβ (10ng/ml) - + + + + + + +
MCC950 (10nM) - - + - - - - -
MCC950 loaded nanosystem (10nM) - - - + - - - -
MCC950 (100nM) - - - - + - - -
MCC950 loaded nanosystem (100nM) - - - - - + - -
MCC950 (1μM) - - - - - - + -
MCC950 loaded nanosystem (1μM) - - - - - - - +
B 72h
**
Relative fluorescence
1.5
1.0
0.5
0.0
TGFβ (10ng/ml) - + + + + + + +
MCC950 (10nM) - - + - - - - -
MCC950 loaded nanosystem (10nM) - - - + - - - -
MCC950 (100nM) - - - - + - - -
MCC950 loaded nanosystem (100nM) - - - - - + - -
MCC950 (1μM) - - - - - - + -
MCC950 loaded nanosystem (1μM) - - - - - - - +

645